Supplementary Information

Moisture-resistant and room-temperature self-healing glassy plastic with thiocarbonyl and hyperbranched structure

Weihang Li,[1a] Minjie Cai,[1a] Yihang Yao,[b] Yue Huang,[a] Haitao Wu,[a] Wenqiang Wu,[a] Jie Wen, [a] Jinrong Wu[a]*

[1]: These authors contribute equally to the work.

[a]: State Key Laboratory of Polymer Materials Engineering, College of Polymer Science and Engineering, Sichuan University, Chengdu 610065, P. R. China.

[b]: Nanostructures for Electronics & Electromechanics Laboratory, School of Engineering, Westlake University, Hangzhou 310024, P. R. China.

*Corresponding author E-mail: wujinrong@scu.edu.cn.

Table of Contents:

1. Materials and methods

1.1. Materials

1,1-thiocarbonyldiimidazole (TCDI, 95+%), Bis(hexamethylene)triamine (BHMT, 98+%), *N,N*-dimethylformamide (DMF, safe dry), deuterated dimethyl sulfoxide (DMSO-d6) and deuterated ethanol were purchased from Adamas. Diethanolamine (DEA, 99%) and Methyl isothiocyanate(MITC, 98%) were purchased from Aladdin. Methanol was purchased from Tansoole Company (China). All reagents and solvents were used without further purification.

1.2. Synthesis of MRGP

The synthetic routes for the moisture resistant glassy polymers (MRGP) are described in detail as follows. In a single-necked round bottom flask, TCDI (0.04 mol, 7.13 g) dissolved in 40 mL DMF was firstly added, and BHMT (0.02 mol, 4.31 g) dissolved in 45 mL DMF was then dropped extremely slowly into the solution with stirring rapidly during the period. The mixed solution of TCDI and BHMT reacted for 1 h at 25 °C under magnetic stirring, during which N_2 was pumped into the flask through a puncture needle. After that, the solution was heated to 40 °C and stirred for 4 h to complete the branching reaction. Next, DEA (0.02 mol, 2.10 g) dissolved in 30 mL DMF was added to the flask and stirred at 40 °C for 1 h. Then, MITC dissolved in 30 ml DMF (0.0405 mol, 3.0 g) was added, and the temperature was raised to 60 °C for 1 h reaction. The resulting solution was slowly poured into a Teflon beaker containing 1 L methanol and stirred at room temperature until the product was completely precipitated. The precipitate was washed 3 times in methanol and dried in a vacuum oven at 40 °C for 24 h and then at 60 °C for 12 h.

1.3. Preparation of the MRGP samples

During this process, the dried MRGP is crushed in a universal crusher and then hot pressed in a Teflon-coated mold at 90 °C and 8 MPa for 5 min. The final product is a pale yellow and transparent dumbbell or rectangular piece or plate.

2. Characterization

2.1. General Characterization

Mass spectra were obtained on a Waters ZQ2000 mass spectrometer in positive ion mode and ionized with an electrospray ionization source (ESI).ATR-FTIR spectra

were recorded on Nicolet iS10 (Nicolet, America) in the range of 4000-500 cm^{-1} at room temperature and 16 scans were performed at the resolution of 4 cm^{-1}. The ^{1}H NMR and ^{13}C NMR spectra of MRGP was measured on a Bruker AV III HD spectrometer operating at 400 MHz in DMSO-D6 with TMS as reference. The dynamic light scattering (DLS) of MRGP in 0.5 mg/mL DMF solution was measured on the Zetasizer nanoanalyzer (Malvern Masterizer 2000), and the average particle size was obtained. The molecular weight of MRGP was determined by gel permeation chromatography (GPC) using DMF as eluent. The thermal gravimetric analysis (TGA) tests were measured by heating samples from 35 °C to 650 °C at a rate of 10 °C/min on a TG209F1. For the samples, the MRGP-exposed was the sample placed at room temperature and 60~68% relative humidity for 5 days and MRGP-soaked was the sample soaked in deionized water for 2 days at room temperature. X-ray diffraction (XRD) experiments studies on MRGP was carried out on a Rigaku Xray diffractometer (Ultima IV) equipped with parallel beam optics attachment and the scanning speed was 10 °/min. DMA tests were measured on TA Q800 in the tension mode with the sample dimension about $20 \times 5 \times 2$ mm^3. The DMA tests were performed in the temperature scanning mode in the range of -50 °C to 100 °C at a ramping rate of 3 °C/min and a frequency of 1 Hz with a strain amplitude of 30 μm. DSC tests were performed on a Perkin Elmer Diamond 3000 with samples heated from -50 °C to 120 °C at a heating rate of 10 °C/min and then cooling at the same rate. The heating and cooling processes were performed two times. The water contact angle of the surface and section of MRGP was obtained by a DSA25 optical contact angle tester. Mechanical performances were measured on an Instron 5967 tensile tester at room temperature with a strain rate of 10 mm/min. The test samples were dumbbell-shaped samples with dimensions of $50 \times 4 \times 2$ mm^3.

2.2. Temperature-dependent FTIR

The sample in the KBr sheet is placed in a vacuum chamber, dehydrated for 30 min in advance at 100 °C, and then heated from -50 °C to 100 °C at 2 °C/min to collect the temperature-dependent FTIR spectra in transmission mode.

2.3. Broadband dielectric spectroscopy (BDS)

The frequency sweep model used a frequency range of 10^{-1} to 10^7 Hz at each temperature point from -60 to 100 °C with 10 °C intervals, and the temperature

stability was better than 0.1 K. Disk-shaped films with a thickness of 1 mm and a diameter of 10 mm were placed in two parallel electrodes to perform the tests.

2.4. Electric-Hysteresis-Loop (EHL)

The Electric-Hysteresis-Loop was tested using the Premier II piezoelectric test system (Precision materials analyzer) produced by Radiant Technologies, INC. We tested the D-E loop of 0.95 mm thick MRGP sheets by gradually increasing the applied electric field intensity from 10.0 kV/cm to 60.0 kV/cm.

2.5. Self-healing tests

The self-healing tests of MRGP were completed by the following two testing methods: Healing test I and Healing test II.

Healing test I: MRGP was tested using the Anton Paar MCR302 rheometer. For press-induced healing tests, a 0.1 mm thick Teflon disc (with a 1 mm diameter central hole) was sandwiched between two MRGP discs (8 mm diameter and 1 mm thickness) to form an assembled specimen, show in Fig. 3a. The assembled specimen was placed on the base plate, lightly pressed with a vertical indenter, and then annealed at 120 °C for 15 min, so that the upper and lower MRGP discs were well connected through the central hole and integrated. The assembled specimen was then slowly cooled to 25 °C at 2 °C/min, and after stabilizing for 1 min, the indenter was rapidly lifted at a tensile rate of 10 mm/min, resulting in brittle fracture in the interconnected region of the specimen. The fractured surfaces were then reconnected and healed for different time under a constant application of 40 N pressure at 25 °C and 30 °C. The healed specimens were tested with the same tensile rate of 10 mm/min to obtain press-induced healing efficiency.

Healing test II: MRGP was tested using the Instron 5967 tensile tester. In order to measure the healing efficiency at different times at room temperature, a blade was used to mark the crack from the center of the thin neck of dumbbell MRGP specimen and the specimen was then broken off. After dipping the section in ethanol, the section was put together in situ and left to stand for a specified time, as shown in Fig. 3a. After the healing was completed, the Instron 5967 tensile tester was used for tensile testing at a speed of 10 mm/min to obtain data and evaluate the healing efficiency.

3. Theoretical calculation

3.1. All-atom molecular dynamics (MD) simulations

The all-atom molecular dynamic simulations were performed using the Materials Studio 2017R2 based on the COMPASS force field.[1] Materials Studio was used to calculate and generate graphical results. The MRGP-water and HGP-water systems were both composed of 10 hyperbranched polymer molecules and 300 water molecules. MRGP is the material studied in this work, and HGP is the theoretically designed contrast sample. The optimized hyperbranched polymer models constructed for simulation are shown in Fig. S5 and Fig. S6. In the simulation process, the hyperbranched polymer molecules and the water molecules were placed in two stacked and combined vacuum amorphous cells (AC), respectively, as shown in Fig. S7. The combined AC were further compressed to bring the polymer and water molecules into contact. The NVT and NPT ensembles were alternatively used at 300 K and 1 bar condition, and NVT ensemble was finally carried out at 300 K to obtain a more equilibrated system. All the dynamic process was hold for 1 ns. The MRGP-water and HGP-water systems underwent the same simulation process.

3.2. Radial distribution function (RDF) calculations.

The radial distribution function (RDF) is used to describe the probability of an atom occurring within the radius r to $r + dr$ of another atom.[2] The hydrogen bonds formed by O atom (proton acceptor) on H_2O molecules and H atom (proton donor) attached to N atom on MRGP or HGP molecules were selected during the calculation. The systems followed the above MD simulations, and additionally, the hyperbranched polymer and water molecules were fully mixed in AC and calculated under NVT ensemble at 500 K for 500 ps to obtain well-equilibrated systems. The RDFs were calculated according to the dynamic of last 1 ns.

3.3. Self-healing efficiency.

Self-healing efficiency (η) is calculated according to the following equation:[3]

$$\eta = \frac{\sigma_{heal}}{\sigma_{ori}} \times 100\%$$

where σ_{heal} is the mechanical property value of the healed samples, and σ_{ori} is the corresponding mechanical property value of the original samples. Mechanical properties here include fracture force, tensile strength and Young's modulus.

3.4. Noda's rules for the 2D correlation spectra (2DCOS).

If the correlation peak Φ (*v1, v2*) in synchronous map shows the same symbol (positive red or negative blue) as the correlation peak Ψ (*v1, v2*) in asynchronous map, then the movement of band *v1* is prior to or earlier than that of band *v2*, and vice versa. Besides, if the correlation peak in synchronous map is not zero (or blank), but zero in asynchronous map, then the movements of bands at *v1* and *v2* are simultaneous. Noda's rules are summarized as follows:[4]

(1) If Φ (*v1, v2*) > 0, Ψ (*v1, v2*) > 0 or Φ (*v1, v2*) < 0, Ψ (*v1, v2*) < 0, then the movement of v1 is before than that of v2.

(2) If Φ (*v1, v2*) > 0, Ψ (*v1, v2*) < 0 or Φ (*v1, v2*) < 0, Ψ (*v1, v2*) > 0, then the movement of v1 is after than that of v2.

(3) If Φ (*v1, v2*) > 0, Ψ (*v1, v2*) = 0 or Φ (*v1, v2*) < 0, Ψ (*v1, v2*) = 0, then the movements of v1 and v2 are simultaneous.

Φ (*v1, v2*) and Ψ (*v1, v2*) represent the correlation peaks in synchronous and asynchronous map, respectively.

3.5. Havriliak-Negami (H-N) equation fitting:

To quantitatively analyze the relaxation processes, the analyses of the dielectric spectra are made by using Havriliak-Negami (H-N) function. In this model, the frequency dependence of the complex dielectric permittivity (ε^*) can be described by the following equation:[5,6]

$$\varepsilon^*(\omega) = \varepsilon_\infty + \frac{\Delta\varepsilon}{\left[1 + (i\omega\tau_{HN})^\alpha\right]^\beta}$$

where $\Delta\varepsilon = \varepsilon_s - \varepsilon_\infty$ is the dielectric strength, ε_s and ε_∞ are the relaxed and unrelaxed values of dielectric constant, and τ_{HN} is the characteristic relaxation time. The parameters α and β ($0 < \alpha$, $\alpha\beta \leq 1$) define the symmetrical and asymmetrical broadening of the dielectric loss peak.

The relation between τ_{HN} and average relaxation time τ_{max} is given by the following equations:

$$\tau_{max} = \tau_{HN}[sin\frac{\pi\alpha\beta}{2(1+\beta)}]^{\frac{1}{\alpha}}[sin\frac{\pi\alpha}{2(1+\beta)}]^{-\frac{1}{\alpha}}$$

$$f_{max} = \frac{1}{2\pi\tau_{max}}$$

where f_{max} is the frequency at which ε'' passes through the maximum value.

3.6. Vogel-Fulcher-Tamman (VFT) equation fitting:

The average relaxation times τ_{max} can be extracted from the H-N equation. This characteristic relaxation time can be correlated with the temperature from 60 °C to 100 °C through Vogel-Fulcher-Tamman (VFT) equation as follows:[7,8]

$$\tau_{max} = \tau_0 \exp\left(\frac{B}{T - T_0}\right)$$

where τ_0 and B are empirical parameters and T_0 is the so-called Vogel temperature.

Further extrapolate the equation to around 25 °C to get the corresponding τ_{max} at room temperature.

3.7. Arrhenius equation fitting:

We use the logarithmic data points of the Arrhenius equation for linear fitting to obtain the activation energy E_a of the relaxation process at a specific temperature. The equation is as follows:[9]

$$\tau_{max} = \tau_0 \exp\left(\frac{E_a}{RT}\right)$$

where τ_{max} average relaxation time at the certain temperature, and τ_0 is a proportionality constant.

3.8. Dielectric property calculation

In order to prove the potential application of MRGP in dielectric materials, the dielectric property parameters of MRGP are calculated here. We use the D-E curves of MRGP to calculate its discharge efficiency (η) according to the following equation:[10]

$$\eta = \frac{S_I}{S_I + S_{II}}$$

where S_I and S_{II} are the areas of part I and part II of the D-E curve (Fig. 5b).

Then the discharge energy density (U_e) of linear dielectric MRGP is calculated by the following equation:[10]

$$U_e = 0.5\epsilon_r\epsilon_0 E^2$$

where ϵ_r is the dielectric constant of the material, ϵ_0 (=8.85×10^{-12} F/m) is the dielectric constant of the vacuum, and E is the applied field strength.

4. Supplementary Figures

a AB₂ intermediate (*M*$_w$: 362)
The terminal groups were converted to thiocarbamates in methanol solution

c Imidazole (*M*$_w$: 68)
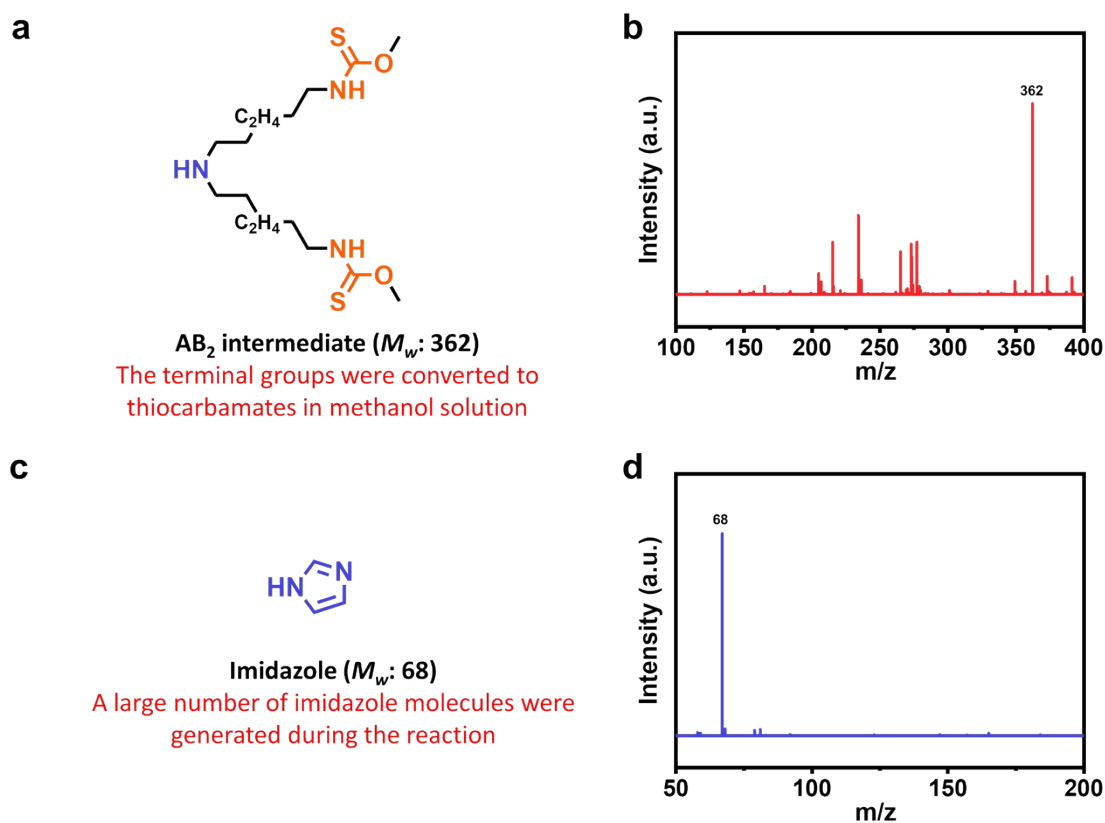A large number of imidazole molecules were generated during the reaction

Fig. S1 Molecular structure diagrams of (a) AB$_2$ intermediate preserved in methanol and (c) imidazole molecule produced by the reaction, and corresponding mass spectra (b) and (d), respectively.

Note: The AB$_2$ intermediates in the form of thiocarbamates were synthesized by mixing TCDI (dissolved in DMF) with BHMT (dissolved in methanol) in an ice bath, with which imidazole molecules were generated. In large amounts of methanol, the thiocarbonyl imidazole terminal groups of the AB$_2$ intermediate were converted to thiocarbamates to prevent further self-polymerization.
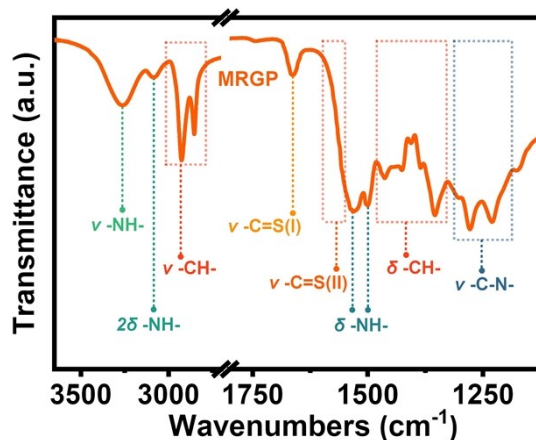
Fig. S2 The FTIR spectra of MRGP.

Note: We confirm the synthesis and structure of MRGP by FTIR. The chemical structure of MRGP mainly consists of methyl thiocarbamate as the terminal group, hexamethylene aliphatic chains and thiourea groups located at the branching points. The peak at 1662 cm^{-1} in the FTIR spectrum is the tensile vibration peak v-C=S (II) of the thiocarbamate bond.[11,12] The tensile vibration peak v-C=S (II) of thiourea is buried at 1575 and 1440 cm^{-1} on the FTIR spectra.[13] It is worth noting that the two broad peaks in the 3600-3000 cm^{-1} region are the vibration band of the -NH- group in MRGP, and the corresponding broad peak at the peak of 3260 cm^{-1} is the tensile vibration peak of -NH- (v-NH-). The peak of 3085 cm^{-1} is the -NH- bending vibration peak (2δ-NH-) in the non-linear thiourea/ thiocarbamate group, which is considered to be the evidence for the formation of non-linear random hydrogen bonds by thiourea/ thiocarbamate groups.[14,15]
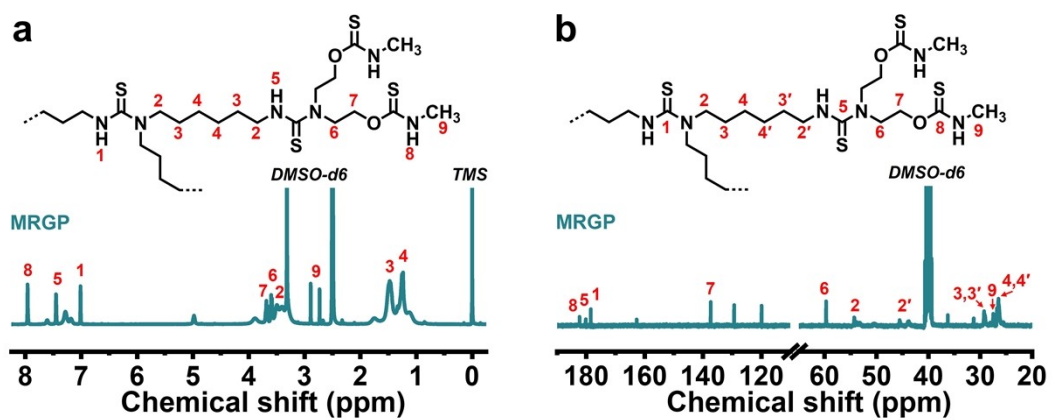
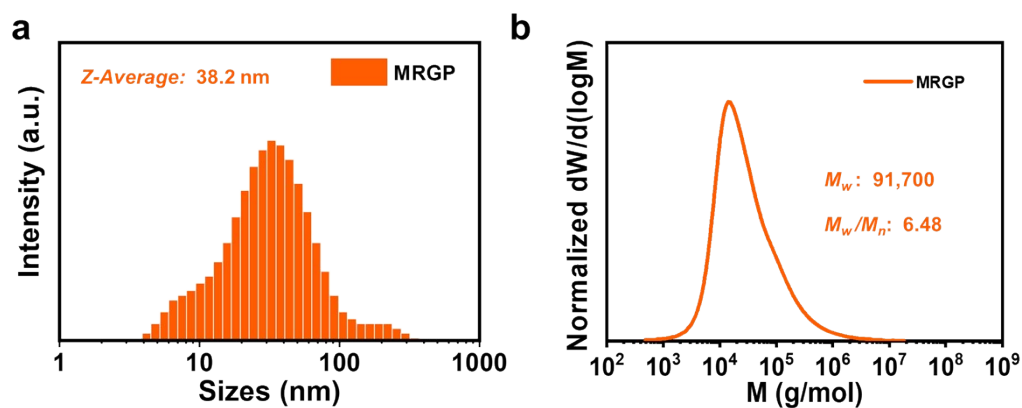**Fig. S3** The (a) ¹H NMR and (b) ¹³C NMR spectra of MRGP and its ideal molecular structure.

Fig. S4 (a) Size distribution, (b) average molecular weight and polydispersity of MRGP.

Note: The DLS test shows that the molecular dynamics average particle size of MRGP in DMF is 38.2 nm, and the GPC result shows that its weight average molecular weight is 91700 (Fig. S4), indicating that MRGP is an independent non-crosslinked hyperbranched macromolecule.[16]
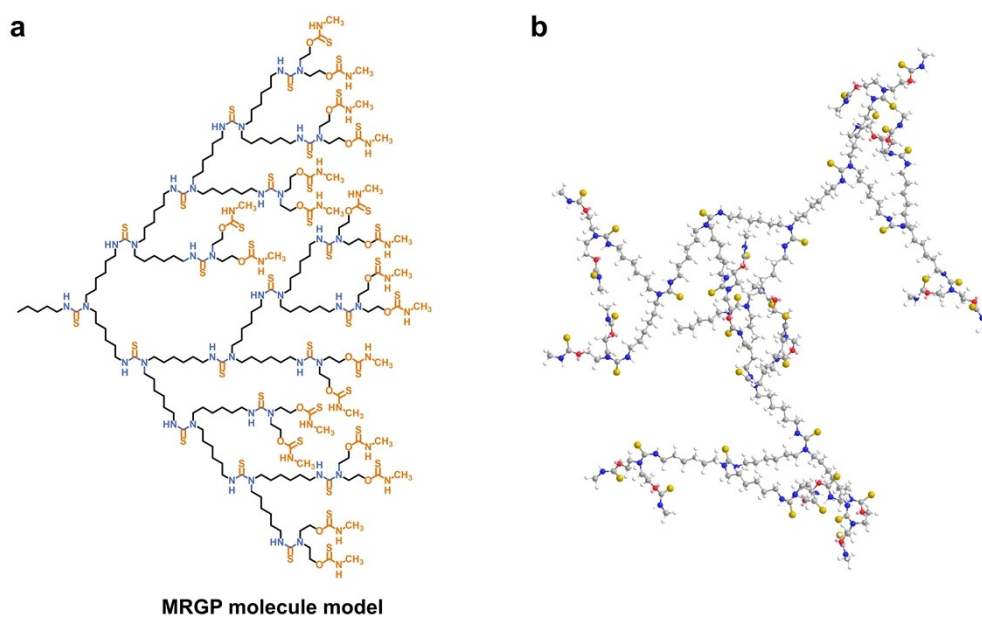
a

MRGP molecule model

b

Fig. S5 (a) Optimized molecular structure of MRGP for simulation. (b) Equilibrated configuration of single MRGP molecule.

a

b

HGP molecule model

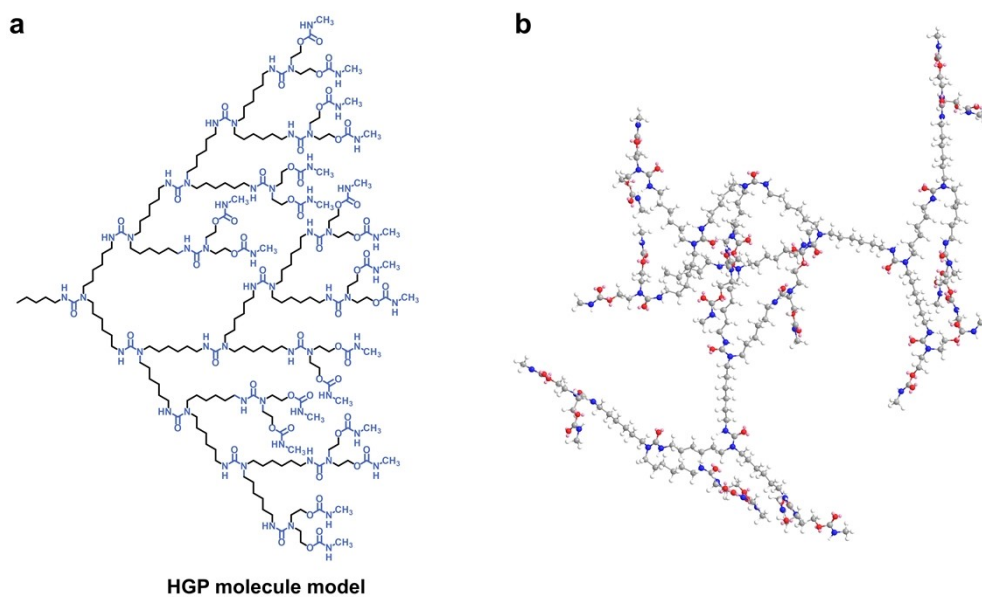**Fig. S6** (a) Optimized molecular structure of HGP for simulation. (b) Equilibrated configuration of single HGP molecule.
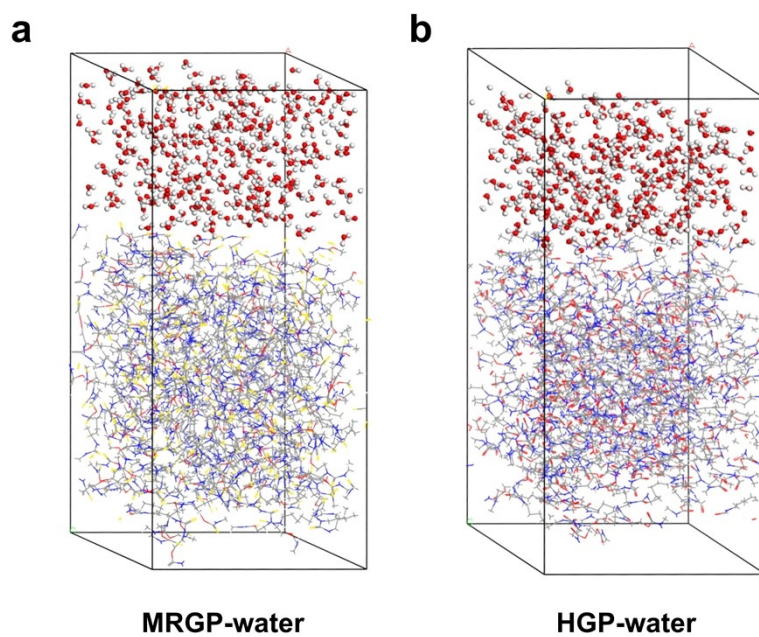
a MRGP-water

b HGP-water

Fig. S7 The status of MRGP-water and HGP-water systems before all-atom MD simulations. Combined amorphous cells containing (a) MRGP-water system: 10 MRGP molecules with 300 water molecules and (b) HGP-water system: 10 HGP molecules with 300 water molecules, respectively.
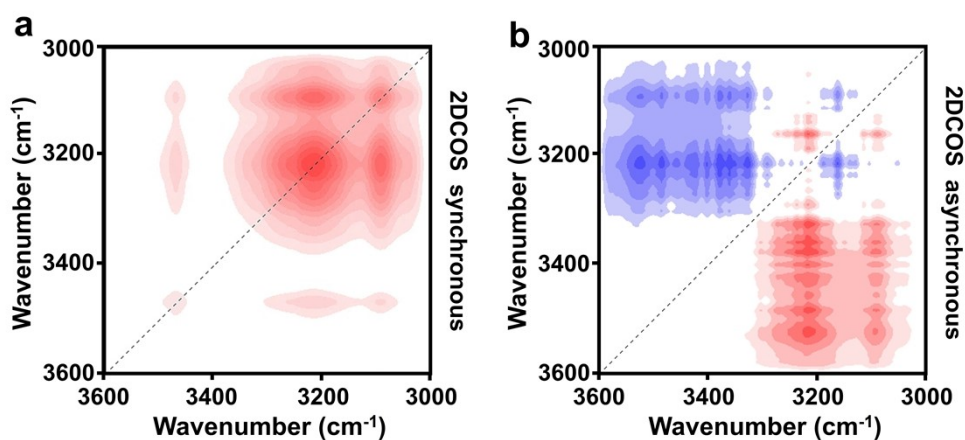
Fig. S8 2DCOS (a) synchronous and (b) asynchronous maps with wavenumber range of 3600-3000 cm^{-1}. The temperature range is between -20~30 °C.

Note: We investigated 2D correlation spectra (2DCOS) analysis of MRGP within a temperature range of -20~30 °C, which is below its T_g. Fig. S8 displays the synchronous and asynchronous maps, where three cross peaks emerge along the diagonal of synchronous map (Fig. S8a) within the range of 3600-3200 cm^{-1}. These peaks correspond to free v-NH-, bound v-NH-, and 2δ-NH- from high to low wavenumbers. By examining the asynchronous map (Fig. S8b) based on the Noda's rule, we can draw the following conclusions. The changes in correlation peaks at [3435, 3260 cm^{-1}] and [3435, 3085 cm^{-1}] indicate that the peak intensity alteration of free -NH- occurs subsequent to that of bound -NH-. Notably, there is no significant correlation peak near [3260, 3085 cm^{-1}] in the asynchronous map, further suggests that the dissociation of linear and non-linear hydrogen bonds in the thiocarbamate/thiourea hydrogen bond network is nearly simultaneous. Moreover, the -NH- group in the bound state converts to the free state subsequent to hydrogen bond dissociation.
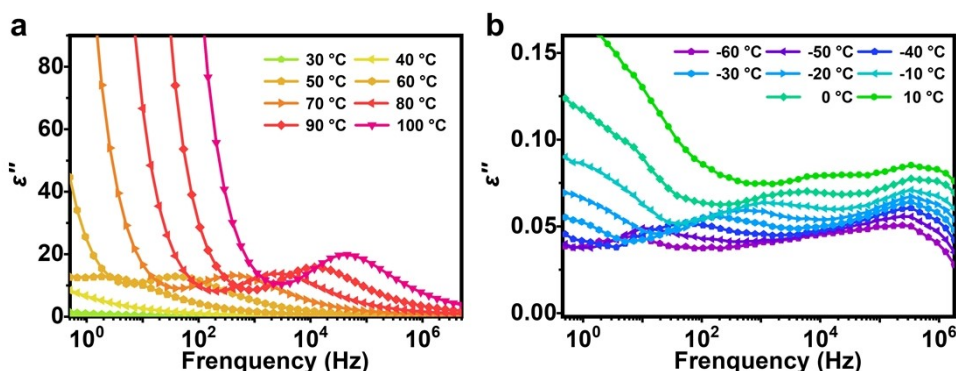
Fig. S9 (a) Dielectric loss ε'' as a function of frequency for MRGP from 30 °C to 100 °C. (b) Dielectric loss ε'' as a function of frequency from -60 °C to 10 °C.

Note: We studied the molecular chain dynamics of MRGP using broadband dielectric spectrometer (BDS) in the wide frequency range of $10^{-1} \sim 10^7$ Hz. Over the glass transition temperature, a primary α relaxation peak appears on the dielectric loss ε'' relaxation spectrum (Fig. S9a), which moves towards high frequency with temperature. The rising DC conductivity curves caused by dielectric polarization will cover other characteristic peaks of the relaxation process except the primary α relaxation.[17] Below the glass transition temperature (-60~10 °C), multiple partially overlapped relaxation processes were observed (Fig. S9b).

5. Reference

1   H. Sun, *J. Phys. Chem. B*, 1998, **102**, 7338-7364.

2   M. Khatib, O. Zohar, W. Saliba, S. Srebnik and H. Haick, *Adv. Funct. Mater.*, 2020, **30**, 1910196.

3   W. Li, H. Liu, H. Wang, Y. Chen, Y. Peng, H. Wu, Y. Hou, Y. Huang, Z. Yuan and B. Ye, *Chem. Mater.*, 2023, **35**, 682-691.

4   B. Sun, Y. Lin, P. Wu and H. W. Siesler, *Macromolecules*, 2008, **41**, 1512-1520.

5   A. Boersma, J. Van Turnhout and M. Wübbenhorst, *Macromolecules*, 1998, **31**, 7453-7460.

6   R. Diaz-Calleja, *Macromolecules*, 2000, **33**, 8924-8924.

7   P. Ortiz-Serna, R. Díaz-Calleja, M. Sanchis, G. Floudas, R. Nunes, A. Martins and L. Visconte, *Macromolecules*, 2010, **43**, 5094-5102.

8   Z. Tang, L. Zhang, W. Feng, B. Guo, F. Liu and D. Jia, *Macromolecules*, 2014, **47**, 8663-8673.

9   M. Menzinger and R. Wolfgang, *Angew. Chem. Int. Ed. Engl.*, 1969, **8**, 438-444.

10   S. Wu, W. Li, M. Lin, Q. Burlingame, Q. Chen, A. Payzant, K. Xiao and Q. Zhang, *Adv. Mater.*, 2013, **25**, 1734-1738.

11   W. Ge, B. Zhao, W. Liu, K. Nie and S. Zheng, *Macromol. Rapid Commun.*, 2021, **42**, 2000718.

12   T. Tian, R. Hu and B. Z. Tang, *J. Am. Chem. Soc.*, 2018, **140**, 6156-6163.

13   J. Liu, C. Jin and C. Wang, *J. Colloid Interface Sci.*, 2020, **561**, 449-458.

14   R. Custelcean, M. G. Gorbunova and P. V. Bonnesen, *Chem. Eur. J.*, 2005, **11**, 1459-1466.

15   Y. Yanagisawa, Y. Nan, K. Okuro and T. Aida, *Science*, 2018, **359**, 72-76.

16   A. Kavand, N. Anton, T. Vandamme, C. A. Serra and D. Chan-Seng, *J. Control. Release*, 2020, **321**, 285-311.

17   M. Sun, S. Pejanović and J. Mijović, *Macromolecules*, 2005, **38**, 9854-9864.